Lessons from fMRI about Mapping Cortical Columns

Seong-Gi Kim and Mitsuhiro Fukuda

Neuroscientist 2008; 14; 287 originally published online Nov 7, 2007;
DOI: 10.1177/1073858407309541

Lessons from fMRI about Mapping Cortical Columns

SEONG-GI KIM and MITSUHIRO FUKUDA
Department of Radiology and Neurobiology
University of Pittsburgh, Pittsburgh, Pennsylvania

Recently developed fMRI can map small functional structures noninvasively and repeatedly without any depth limitation. However, there has been a persistent concern as to whether the high-resolution fMRI signals actually mark the sites of increased neural activity. To examine this outstanding issue, the authors used iso-orientation columns of isoflurane-anesthetized cats as a biological model and confirmed the neural correlation of fMRI iso-orientation maps by comparing them with intrinsic optical imaging maps. The results suggest that highest fMRI signals indeed indicate the sites of increased neuronal activity. Now fMRI can be used to determine plastic and/or developmental change of functional columnar structure possibly on a layer-to-layer basis. In this review, the authors focus mainly on what technical aspects should be considered when mapping functional cortical columns, including imaging techniques and experimental design. NEUROSCIENTIST 14(3):287–299, 2008. DOI: 10.1177/1073858407309541

KEY WORDS *Orientation columns, Hemodynamics, High resolution, BOLD, Optical imaging*

Neurons with common functional properties in the mammalian cortex are often clustered into sub-millimeter-scale columns, which span the entire cortical plate (Mountcastle 1957; Hubel and Wiesel 1962). Although a direct relationship between this clustering and function is repeatedly questioned (Swindale 1990; Purves and others 1992; Horton and Adams 2005), the structure, function, and plasticity of cortical columns have no doubt been of great interest. Thus, many efforts are dedicated to visualizing functional structures. Initially, the existence of cortical columns was determined by single-unit recordings (Hubel and Wiesel 1962, 1963). Because unit recordings measure on a point-by-point basis, it takes an enormous time to record a sufficient number of neurons to obtain a partial picture of columnar arrangement. To map cortical columns effectively, techniques must be capable of acquiring high resolution and of covering large cortical areas; 2-deoxyglucose (2-DG) autoradiography and optical imaging meet these requirements. The 2-DG autoradiography measures increases in the glucose consumption rate during stimulation (Kennedy and others 1976). However, in vivo imaging is not possible, and only the map corresponding to one stimulus can be obtained. The first high-resolution mapping of functional columns in live animals was accomplished by Blasdel and Salama (1986) using a video camera and a voltage-sensitive dye. Their seminal study triggered the use of optical signals for mapping functional columns (Tso and others 1990; Bonhoeffer and Grinvald 1991; Grinvald 1992; Malach and others 1993). The optical imaging of intrinsic signals detects a change in reflection of the incident light through the cortex, induced by a change in light-absorbing hemoglobin contents (Grinvald and others 1986; Frostig and others 1990). Because endogenous hemoglobin is used as a tracer, it allows mapping during repeated measurements. Even though this technique has been used extensively for mapping columnar structures, its application is limited to the upper layers of exposed cortex due to a limited penetration of light and to animal models due to the required invasive surgical preparation. An extension of mapping functional columns to humans awaits the progress of recently developed fMRI. Using high-resolution fMRI, ocular dominance column–like maps in humans have been obtained by subtracting images acquired during right-eye-only and left-eye-only stimulation (Menon and others 1997; Menon and Goodyear 1999; Cheng and others 2001; Goodyear and Menon 2001).

Setting aside the biological meaning of functional columns, the columnar structure is an ideal biological model to evaluate the spatial resolution of functional imaging techniques. There has been a persistent concern as to whether the high-resolution fMRI signals actually mark the sites of increased neural activity. This skepticism is based not only on a lack of a direct confirmation by other techniques but also because of possibly a broad point spread function (PSF) of hemodynamic-based fMRI signals. Although an increase in fMRI signal is closely correlated with an increase in neuronal activity on a large supramillimeter scale (Heeger and others 2000; Logothetis and others 2001), this finding may not be applicable on a submillimeter columnar scale (Duong and others 2000; Cheng

The authors thank Ping Wang for animal preparation, Michelle Tasker for proofreading and animal preparation, and Chan-Hong Moon for providing BOLD data. This work was supported by the NIH (NS44589, EB003324, EB003375).

Address correspondence to: Seong-Gi Kim, 3025 East Carson Street, Pittsburgh, PA 15203; e-mail: kimsg@pitt.edu.

ISSN 1073-8584

and others 2001; Kim and others 2004). Thus, it is critical to examine whether fMRI can pinpoint sub-millimeter functional sites. This outstanding issue motivates us to study reproducibility, specificity, and confirmation of fMRI columnar maps (Fukuda and others 2006a; Moon and others 2007). To do this, we selected a well-established orientation column model in cats, which has been extensively investigated by single-unit recordings, 2-DG autoradiography, and optical imaging of intrinsic (OIS) signals (Payne and Peters 2002). This review focuses mainly on what technical aspects should be considered when mapping orientation columns using fMRI.

Vascular Physiological Changes Induced by Neural Activity

Because fMRI measures vascular hemodynamic responses induced by increased neural activity, it is important to understand the chain of events from task to fMRI signals. Task and/or stimulation induce neural activities at localized regions, which will trigger an increase in the cerebral metabolic rate of oxygen ($CMRO_2$), cerebral blood flow (CBF), and cerebral blood volume (CBV). Because $CMRO_2$ change occurs in neuronal active tissue (Thompson and others 2003) and precedes vascular responses (Ances and others 2001; Shibuki and others 2003), its measurement will provide the high spatial specificity (Malonek and Grinvald 1996). On the contrary, CBF and CBV are vascular parameters; CBF is defined as milliliters (mL) blood delivered to the region of interest per gram (g) of tissue and per minute, whereas CBV is an intraluminal space of blood vessels within the region of interest (unit of mL blood per g tissue). Typically, gray matter in normal humans has CBF of 50 to 70 mL/100 g/min and CBV of 2 to 5 mL/100 g (Leenders and others 1990). When CBF is measured by a diffusible tracer such as water, the change in blood flow can be observed in both vasculature and tissue (i.e., extra-vasculature). Both CBF and CBV are physiological parameters independent of imaging techniques.

It is thought that neural activation leads to an increase in oxygen delivery without a commensurate elevation in cerebral oxygen consumption (Fox and Raichle 1986; Fox and others 1988), which results in hyperoxygenation and a decrease in the capillary and venous deoxyhemoglobin (dHb) contents (see Fig. 1 for a schematic). Because dHb acts as an endogenous paramagnetic contrast agent (Pauling and Coryell 1936), a decrease in the local dHb content in the brain induced by neural activity leads to an increase in the intensity of the MRI signal (Ogawa and others 1990a, 1990b; Ogawa and Lee 1990). This imaging contrast is dubbed the "blood oxygenation level–dependent" (BOLD) contrast, originating from small and large venous vessels and neighboring tissue (Ogawa and others 1990a). The BOLD fMRI technique has been widely used because of its high sensitivity and easy implementation. The BOLD signal is dependent on various anatomical, physiological, and imaging parameters (Ogawa and others 1993).

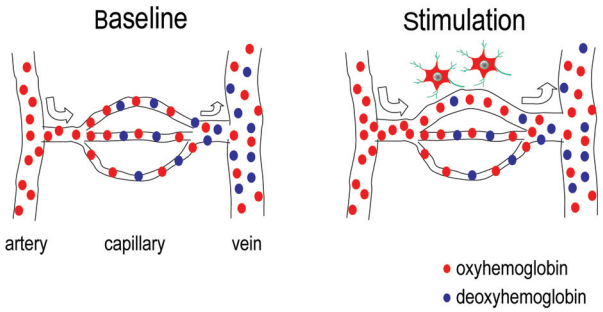

Fig. 1. A schematic of vascular responses induced by neural activity. Blood containing oxyhemoglobin (red circles) and/or deoxyhemoglobin (blue circles) travels from arteries, arterioles, capillaries, venules, and finally to veins. Oxygen delivered via oxyhemoglobins diffuses into (extravascular) tissue and is used as metabolic substrates. At prestimulus baseline conditions, blood oxygen saturation is close to 100% in arteries, whereas it is ~60% in veins (even though it varies depending on the subject's physiological condition). When neural activities increase, they will trigger an increase in blood velocity (indicated by the size of arrows) and dilation of the vessels directly or indirectly. Because the cerebral blood flow increase induced by an increase in neural activity overcompensates for an increase in the oxygen consumption rate, venous blood is more oxygenated during stimulation (i.e., more oxyhemoglobin and less deoxyhemoglobin contents). Partially deoxygenated blood will drain from the capillaries to the large veins.

Sensitivity and Specificity of Hemodynamic-Based fMRI

To obtain high-resolution fMRI, two major issues have to be considered: sensitivity of techniques and specificity of the signal source (i.e., the spatial extent of the signal at the site of neuronal activity). Both factors will determine the accuracy of the functional map. High-resolution fMRI suffers from poor sensitivity. For example, a voxel dimension of $0.15 \times 0.15 \times 1$ mm^3 for our high-resolution fMRI is 1200 times smaller than the $3 \times 3 \times 3$-mm^3 resolution used in typical human studies and requires 1200^2 more averages to achieve similar sensitivity with the same equipment. Thus, it is crucial to optimize fMRI hardware and software as well as the stimulation paradigm and data analysis to maximize the sensitivity. Because sensitivity increases are roughly linearly dependent on magnetic field strength and inversely related to receiver coil size, an ultrahigh magnetic field of 9.4 Tesla and a small coil of 1.6 cm diameter were mostly used for our cat orientation column studies (note that 1 Tesla is equivalent to 10,000 gauss, and Earth magnetic field is 0.5 gauss). What signal source should then be measured with fMRI to achieve a high spatial specificity?

Considering spatially well-localized metabolic responses, measurement of $CMRO_2$ changes can provide a high specificity of fMRI signals. Because stimulation-induced

$CMRO_2$ change precedes CBF and CBV responses, hypooxygenation may be initially experienced until the CBF response catches up with $CMRO_2$ demand. Optical imaging of intrinsic signals showed that the initial increase of "metabolism-based" deoxyhemoglobin signal (Vanzetta and Grinvald 1999) can be used to resolve functionally active, individual orientation columns in the cat visual cortex (Malonek and Grinvald 1996). An early increase in dHb contents will lead to the early negative BOLD signal (referred to as an "early dip") (Kim and others 2000), which likely indicates an early oxygen consumption change (Nagaoka and others 2006). However, to detect this early BOLD response and use the high spatial specificity of the early dip signal, images must be acquired with high spatial and temporal resolution, which results in a significant reduction in sensitivity. Therefore, the measurement of early dip is not practical. Alternatively, hemodynamic-based responses (i.e., positive BOLD, CBV, CBF) should be considered for high-resolution fMRI.

The specificity of hemodynamic-based fMRI signals is dependent on both vascular regulation and the sensitivity of the imaging technique to different vessel types and sizes. To obtain high-resolution fMRI with high specificity, it is important to obtain signals from microvessels such as capillaries and/or tissue, not from large vessels. The microvasculature signal is believed to be close to the site of increased neural activity (e.g., distance between capillaries and neurons is < 25 μm because an average intercapillary distance is ~ 25 μm [Pawlik and others 1981]), whereas functional maps based on the macrovasculature can be significantly distant from the actual site of neuronal activity.

The conventional positive BOLD fMRI signal is sensitive to all sizes of venous vessels and surrounding tissue. The principal intracortical veins with an average of ~100 μm diameter, which lead directly to the cortical surface, drain blood from surrounding capillaries up to 2 mm away, and intermediate-size veins (with <80 μm diameter) drain up to 0.5 mm (Duvernoy and others 1981). Because conventional BOLD signals are sensitive to changes in these large intracortical veins, its spatial resolution is limited by the density of large vessels and the extent of draining effects. To obtain columnar-resolution functional images, the signal from large vessels should be minimized using postprocessing techniques and improved data acquisition methods. Postprocessing approaches detect large draining vessels by using various BOLD signal characteristics such as a large intensity (Kim and others 1994) or a delayed response (Lee and others 1995). Although these subjective criteria are effective (Cheng and others 2001), it may not be sufficient to detect and remove all large-vessel contaminations. Remaining "common" large-vessel contributions to the BOLD signal can be removed by the differential imaging approach if functional territories are complementary during orthogonal stimuli (Menon and others 1997; Cheng and others 2001). However, this differential method cannot be used in most fMRI studies because of unknown orthogonal stimulation conditions. Thus, it is critical to remove or minimize the draining vessel contribution during data acquisition. For this, perfusion-based techniques can be used because of their high sensitivity to changes in capillaries and tissue.

CBF measurements have been extensively performed using ^{15}O-labeled water as an exogenous positron emission flow tracer, although inherent resolution limitations due to sensitivity, positron travel distances, and detector arrangements prevent sub-millimeter imaging. Alternatively, CBF-weighted images can be obtained using MRI by employing arterial blood water as an endogenous flow tracer. Arterial spin labeling (ASL) can be achieved by radiofrequency pulse(s), and then magnetically labeled spins move into capillaries in the imaging slice and exchange with tissue water spins. Because a background water signal exists, it is important to remove non-flow-related water signals. Thus, 2 images are typically acquired: one with arterial spin labeling and the other without labeling (Detre and others 1992; Edelman and others 1994; Kim 1995; Kwong and others 1995). The difference between the 2 images is directly related to CBF, and relative CBF changes due to physiological perturbations can be measured. The perfusion-based signal change as measured by MRI predominantly arises from changes in local CBF at the level of arterioles and capillaries/tissues.

Alternatively, an exogenous intravascular contrast agent with high susceptibility can be used in animal studies to improve sensitivity and specificity relative to BOLD fMRI. Dextran-coated iron oxide nanoparticles have been used as a long half-life intravascular susceptibility contrast agent (Kennan and others 1998; Mandeville and others 1998; van Bruggen and others 1998), similar to endogenous irons in dHb molecules (used for the BOLD contrast). The half-life of the iron oxides in blood is dependent on particle size and species; the typical half-life of 20- to 30-nm diameter particles is >4 h in rats (Mandeville and others 1998), 3 to 6 h in cats (in our observation), and >18 h in nonhuman primates (Vanduffel and others 2001). During a steady-state condition established following the infusion of an intravascular contrast agent (reached within a few minutes), an increase in CBV during stimulation will induce an increase in intravoxel contrast agent and, consequently, a decrease in MRI signal. Unlike in the BOLD case, iron oxide concentration in blood does not change with alterations in blood flow and oxygen consumption induced by neuronal activity. Although the change in dHb (used in the BOLD signal) will contribute to the MRI signal, exogenous contrast agents with sufficiently high doses dominate the effect compared to dHb. Thus, fMRI following the injection of contrast agents is predominantly weighted by the CBV change. Small-sized vessels, including precapillary arterioles, dilate rigorously during stimulation, whereas large vessels do not dilate much (Lee and others 2001). Furthermore, the MRI signal is very weak in a voxel containing large vessels due to a large amount of contrast agent, and thus its change induced by dHb changes may not be detected (Mandeville and Marota 1999). Thus, the specificity of CBV-weighted fMRI can be improved to small-sized vessels and surrounding tissue. The sensitivity gain of the CBV measurement over the

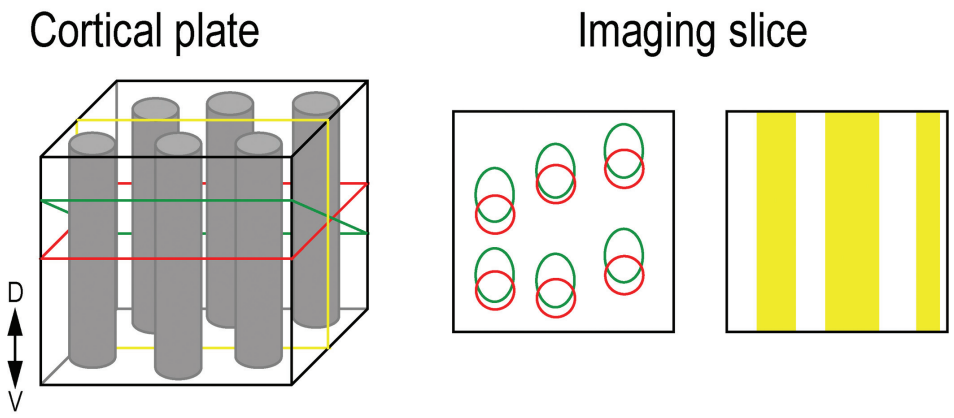

Fig. 2. Schematics of slice selections and apparent patterns of columns. Columns orthogonal to the surface of the cortex run across the entire cortex. Two-dimensional MRI slice(s) can be chosen with a well-defined thickness at an arbitrary angle. Thus, appearance of columns in 2-D images is dependent on the slice selection relative to the column direction. When the imaging slice is orthogonal to the column direction, fMRI patterns are the same as the dorsal view of columns (red circles). If the imaging slice is oblique to the column direction, column patterns elongate depending on the oblique angle and slice thickness (green ovals). If the imaging slice is parallel to the column direction, bar-like patterns appear dependent on slice thickness (yellow bars).

BOLD technique is dependent on the dose of the contrast agent, the imaging parameters, and the magnetic field. When 5- to 15-mg iron/kg body weight is used, the sensitivity gain is about 1.3- to 5-fold (Mandeville and others 1998, 2001; Kim and Ugurbil 2003; Zhao and others 2006).

Experimental Design and Data Analysis

Because MRI is obtained from an imaging plane(s), the selection of an imaging slice relative to column directions will make columnar maps different. Figure 2 shows a schematic of apparent "column" shape in a 2-D image. When the slice direction is perfectly orthogonal to the column direction (see red slice), activation patterns in fMRI appear as circles (red), which are the same as the dorsal view of columns. When the slice direction is oblique to the column direction (see green slice), columnar shapes are elongated and larger than the actual size of the columns. If the imaging slice is parallel to the column direction (yellow slice), columns in 2-D images appear as bars in fMRI maps. Thus, it is crucial to determine the imaging slices properly.

The selection of the imaging slice can be aided by 3-D MRI because the column direction is orthogonal to the surface of the flat cortex. The imaging slice can be selected to parallel the surface of the cortex. Moreover, because columns and intracortical vessels run roughly orthogonal to the cortical surface, the visualization of intracortical vessels can be used. In our studies, a 3-D high-resolution venographic image with ~80 μm resolution was acquired from cat brain (Fig. 3). The voxel containing intracortical veins appears to be hypointense because paramagnetic deoxyhemoglobin gathers into draining venous vessels. Dark spots indicate that intracortical veins run through the plane, whereas dark lines suggest that veins run parallel or obliquely within the imaging plane. The primary visual cortex is located in the marginal gyrus, and thus orientation columns should exist between the midline (dashed and dotted lines) and lateral sulcus (dashed line).

For fMRI studies, isoflurane-anesthetized cats are restrained in a normal postural position using a custom-designed nonmagnetic stereotaxic frame. Visual stimuli consisted of high-contrast square-wave moving gratings (0.15 cycle/degree, 2 cycle/s) of different orientations to elicit neuronal activity in cat areas 17 and 18 (Movshon and others 1978). Two different stimulation paradigms can be used: block design and continuous stimulation paradigms. The conventional block design stimulation paradigm consists of repeated baseline control and orientation stimulation periods (see Fig. 4*A*). Control can be either stationary gratings or stationary solid gray (blank). Temporal resolution of fMRI is limited by hardware of MR equipment and MR physics. After the excitation of water proton spins (for MRI data collection), these spins will return to a normal status, which takes typically 1 to 3 s, depending on magnetic field strength and tissue type. Thus, rapid repetitions of excitations will significantly reduce the sensitivity of MR signals due to insufficient recovery from the preceding excitation. In our high-resolution fMRI studies with a temporal resolution of 2 to 6 s, a 10- to 60-s stimulation duration was used for obtaining a sufficient number of data points in each period. Data analysis can be performed by simple subtraction of the averaged control image from the averaged stimulated image or by using general linear models. This simple analysis produces "single-condition" functional maps. When the orthogonal stimulus condition is known, the differential method can be used by subtraction of the single-condition map induced by one orientation from that induced by the

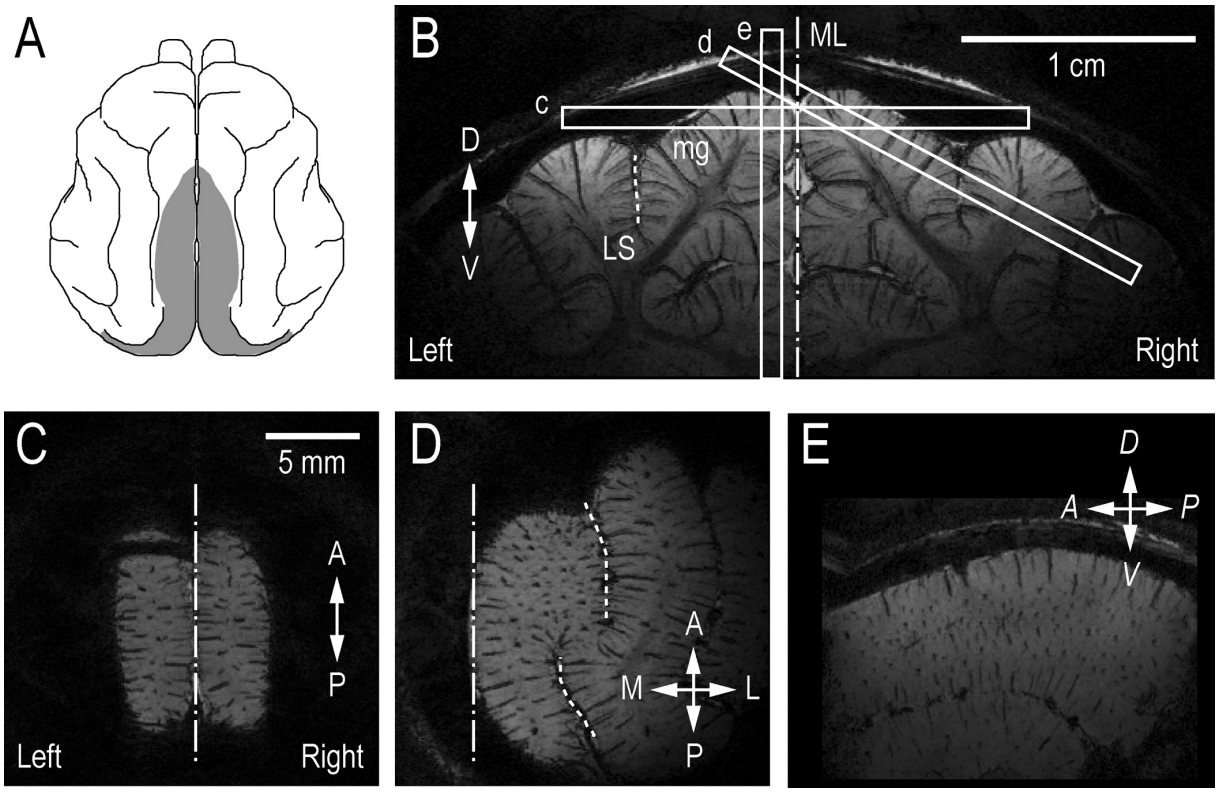

Fig. 3. A sketch of cat brain and 2-D slice view of various imaging slices. In the dorsal view of the cat brain (*A*), the gray area indicates visual areas 17 and 18, where orientation columns are expected to be present. To select imaging slices for columnar mapping, a 3-D venographic image was acquired. From the 3-D image, a 2-D section can be selected for fMRI studies. In the coronal view (*B*), 3 different imaging slices indicated by 1-mm thick slabs can be chosen to cover visual area 17 or 18, transverse (c), oblique (d), and sagittal (e). Corresponding images are shown in *C*, *D*, and *E*. Dark lines or spots indicate venous blood vessels. Most intracortical vessels run nominal to the surface of the cortex. When vessels appear as small dark dots, then the imaging plane is selected roughly orthogonal to the vessel direction. LS (dashed line) = lateral sulcus; ML (dashed and dotted line) = midline; mg = marginal gyrus; D = dorsal; V = ventral; M = medial; L = lateral; A = anterior; P = posterior.

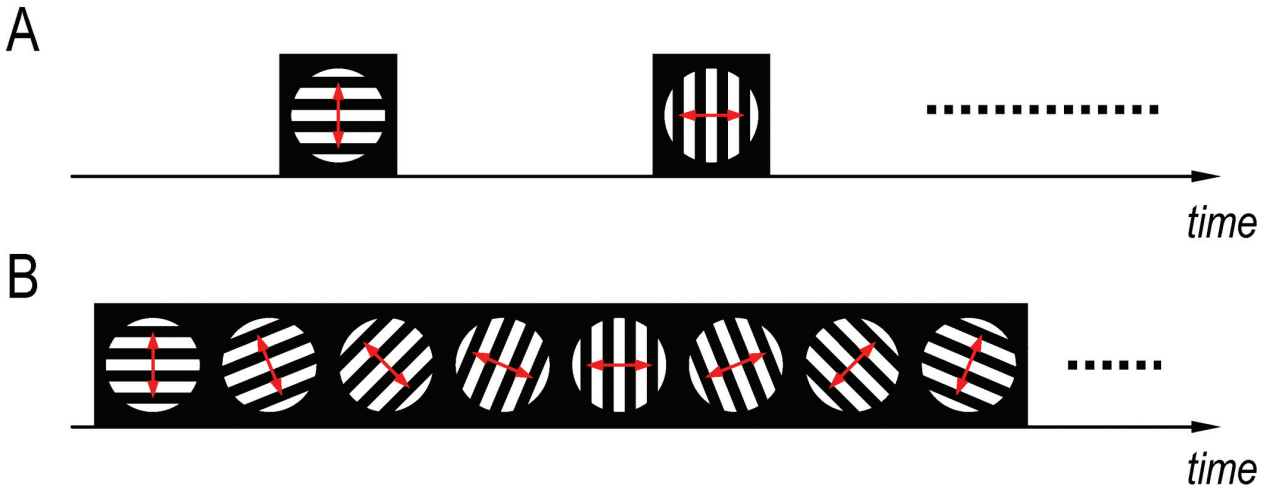

Fig. 4. Stimulation paradigms used for mapping orientation columns. (*A*) Block design. Orientation-selective stimulation period follows prestimulus control period. Red double arrow in black-and-white gratings indicates a direction of motions. The same stimulus may be repeated, or 2 orthogonal stimuli may be interleaved. (*B*) Continuous stimulation paradigm. Orientation-selective stimuli are presented without any control period. In this specific example, 8 different orientations are presented sequentially. Because no control period is used here, total response induced by one orientation cannot be determined, and the difference of signals induced by different stimuli will be observed.

orthogonal orientation (Blasdel 1992; Bonhoeffer and Grinvald 1993) because orthogonal stimuli activate complementary territories. The differential approach has been extensively used by the optical imaging community to image cortical columns (referred to as a *differential map*).

For orientation column mapping, continuous cyclic stimulation without control periods can also be adopted instead of block design stimulation. For example, in our experiments, 8 orientations were presented (0° [horizontal] to 157.5°, 22.5° increments, 10 s each) without gaps between stimuli, and the 80-s cyclical continuous stimulation paradigm was repeated 10 times (see Fig. 4*B*). The fMRI signal can be modeled using sinusoidal functions with multiple-frequency components. Thus, Fourier analysis can be applied to decompose signals continuously recorded for 800 s (10 stimulation cycles) into different temporal frequency components (Engel and others 1997; Kalatsky and Stryker 2003). Then, the orientation-specific signal at a frequency of 0.0125 Hz (i.e., 1/80 Hz) can be used to generate orientation-specific maps. This Fourier method is advantageous over the differential data analysis approach because the fMRI response following the orientation-specific stimulation cycle can be easily separated from other frequency components induced by vasomotion (Mayhew and others 1996), respiration, heartbeat, and so on. The fMRI signal responds to the orientation changes in a gradual manner, which is well fitted by a cosine function model. Thus, the Fourier analysis method with continuous stimulation (Kalatsky and Stryker 2003) is more efficient to detect functional response compared to a conventional block design paradigm (Kim and others 2000; Zhao and others 2005a). However, the hemodynamic response time must be determined to accurately assign an orientation preference to fMRI maps acquired with continuous stimulation because the hemodynamic response is not instantaneous but rather sluggish. Note that the block design paradigm will not have this problem. The hemodynamic response time can be determined using 2 different orientation presentation orders (Kalatsky and Stryker 2003): one is the "forward" direction starting at 0° and increasing in orientation by 22.5°; the other is the "backward" direction starting at 157.5° and decreasing in orientation by 22.5°. The hemodynamic response time is the same in the forward and time-reversed backward stimulation data, but its direction is opposite; therefore, the effect of the hemodynamic response time can be removed from the functional maps.

Intrinsic Spatial Specificity of Hemodynamic Responses

Because the spatial extent of the hemodynamic response will impose a fundamental limitation on the spatial resolution of fMRI modalities, assessment of the intrinsic hemodynamic point spread function (PSF) becomes imperative. According to intrinsic optical imaging studies, the increase in oxyhemoglobin signals, resulting from stimulus-evoked CBF and blood volume increases, was spatially diffuse and extended far beyond the true activation site (Malonek and Grinvald 1996). Based on these findings, it is concluded that the delayed oxyhemoglobin and deoxyhemoglobin signal changes are not sufficiently localized to the actual areas of elevated neuronal activity to resolve cortical orientation columns. However, it is unknown whether the poor spatial specificity in the delayed optical signals is due to intrinsic properties of coupling between neuronal activity and blood flow or, alternatively, contamination from large downstream pial veins or upstream pial arteries. This can be directly examined using CBF- or CBV-weighted fMRI because signal contributions from pial vessels can be avoided by appropriate slice selection, unlike the surface optical imaging techniques.

The CBF-weighted fMRI technique was applied to determine the spatial specificity of CBF responses induced by orientation-selective stimulation (Duong and others 2001). ASL images were acquired in a transverse view using the block design single-orientation stimulation. Figure 5 shows the CBF activation map of one representative animal. Increased CBF activity was observed predominantly in the tissue area, avoiding the superior sagittal sinus (indicated by the arrow). Most important, the CBF functional maps exhibit "patchy" layouts with semiregular cluster shapes in area 18, a prominent topological characteristic of orientation columns, as observed using 2-DG (Lowel and others 1988) and optical imaging (Bonhoeffer and Grinvald 1991, 1993). The time course of fMRI signals within the active regions shows a ~20% increase during 0° stimulation (indicated by 60-s bars). Our data indicate that the previous optical imaging finding of poor CBF specificity is most likely due to large pial vessel contributions. Proper CBF contrast in ASL images is only achieved when enough time is allowed for the labeled arterial water to travel into the region of interest and exchange with tissue water. This makes it difficult to detect changes in CBF with a temporal resolution greater than the lifetime of the labeled water (~1.5–2.3 s). Acquisition of a pair of images can further reduce temporal resolution and, consequently, the signal-to-noise ratio. Also, the selection of CBF-based imaging slices is dictated by the direction of flow. Thus, CBF-based imaging techniques have not been widely used for routine fMRI studies. Similar to the quantitative CBF approach, the CBV-weighted fMRI technique with iron oxide contrast agents may be applied for high-resolution mapping in animals.

CBV-weighted fMRI experiments were performed in a sagittal plane after injection of 10 mg iron/kg body weight using the block design stimulation. Raw stimulation-induced signal change (i.e., poststimulus image minus prestimulus image) maps were obtained without any statistical threshold (illustrated in Fig. 6*A*, *B* for 1 animal of 45° vs. 135° gratings, respectively). Higher CBV increase results in larger negative signal changes. Patchy clusters were observed in complementary territories between single-condition 45° and 135° maps (Fig. 6*A* vs. 6*B*). To enable comparison with previous optical imaging studies (Bonhoeffer and Grinvald 1991, 1993), differential maps (e.g., Fig. 6*C*) were obtained by subtracting the

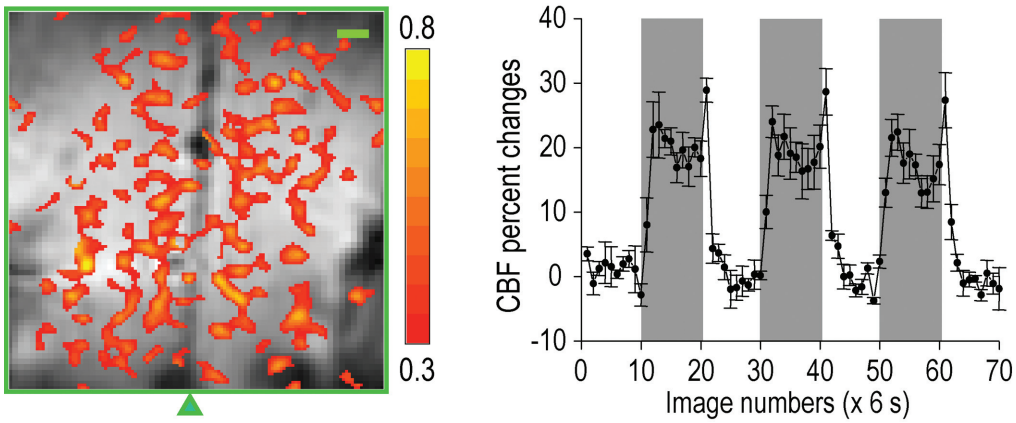

Fig. 5. Perfusion (cerebral blood flow [CBF])–weighted fMRI map corresponding to 0° stimulation and time course of active pixels (Duong and others 2001). An imaging slice was selected in a transverse plane, and arterial spin-labeled images were acquired with a temporal resolution of 6.0 s. The functional map was generated by using cross-correlation analysis between raw time course and a box-car reference function based on the block design stimulation paradigm. The functional map (color) was overlaid on an anatomic image. Color bar, cross-correlation value between 0.3 and 0.8; scale bar, 1 mm; gray bars, stimulation periods.

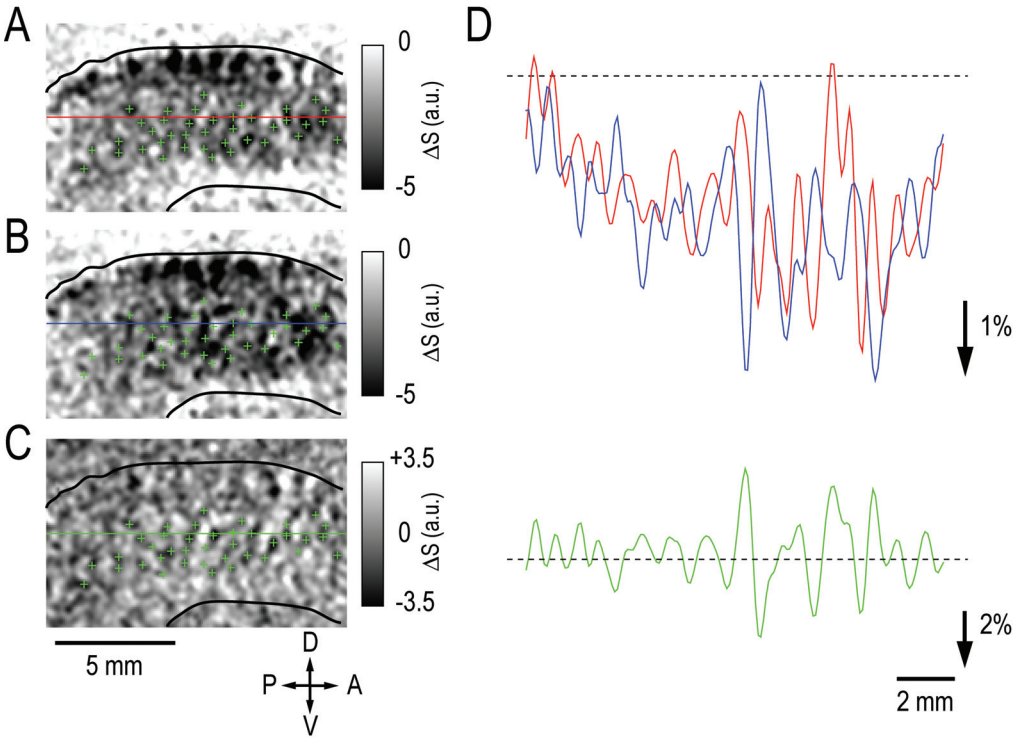

Fig. 6. Cerebral blood volume (CBV)–weighted fMRI. CBV-weighted fMRI was obtained in a sagittal plane after intravascular injection of superparamagnetic iron oxide nanoparticles. Negative signal change indicates an increase in CBV during stimulation. Single-condition maps corresponding to 45° and 135° stimulation (*A* and *B*, respectively) are shown as well as their differential map (*C*). The dorsal contour indicates the edge of the brain, whereas the ventral contour is the splenial sulcus. To easily visualize patches responding to 45°, green plus signs were obtained from the 45° single-condition map and then overlaid on the 135° single-condition map (*B*) and the differential map (*C*). Clearly, functional territories responding to 2 orthogonal stimuli are complementary. Spatial profiles in a posterior-anterior direction indicated by a line were obtained (*D*). Clearly, negative signal changes indicating increases in CBV were observed from baseline (dashed horizontal line). The subtraction of 135° from 45° profiles enhances differential responses induced by 2 orthogonal stimuli; negative peaks represent the regions preferred to the 45° stimulation, whereas positive peaks represent the 135° stimulation. The interval between positive (or negative) peaks is related to intercolumn distance. D = dorsal; V = ventral; A = anterior; P = posterior.

single-condition maps for 2 different orthogonal visual stimuli. In the differential iso-orientation map (Fig. 6*C*), regions sensitive to the 45° orientation ("45° iso-orientation domain") are shown as black, whereas pixels with preferential activity for the orthogonal stimulus ("135° iso-orientation domain") are white. Clearly, patchy clusters preferential to the 2 orthogonal stimuli are segregated. The patterns and shapes of clusters in the differential maps are consistent with those found in intrinsic optical imaging (Bonhoeffer and Grinvald 1993). The average anterior-posterior distance between iso-orientation domains in differential images is 1.37 ± 0.28 mm in all studies (n = 10 hemispheres) (Zhao and others 2005b), which is also consistent with the result using the 2-DG method (Lowel and others 1987). Spatial profiles of signal changes along a single line of the entire field of view in the anterior-posterior direction (indicated by lines) were visualized (Fig. 6*D*). The difference between 2 single-condition profiles is also shown. The average ratio in all studies of CBV changes induced by preferred orientation versus orthogonal orientation gratings is 1.7, indicating that the nonspecific response is quite significant (in other words, 0.7 for orientation specific vs. 1.0 for orientation nonspecific) (Zhao and others 2005b). The non-orientation-specific signals can be due to a contribution from subthreshold synaptic activity in inactive domains (Das and Gilbert 1995), a less-specific CBV response compared to metabolic and neural activity (Malonek and Grinvald 1996), nonoptimal visual stimuli for some populations of neurons (due to the use of only 2 orientations), nonideal slice selection relative to the direction of columnar organization, and/or limited spatial resolution (pixels contain neurons with varying responses to the orientation of stimuli). Combining CBF and CBV data together, we can conclude that hemodynamic-based fMRI techniques per se can indeed be used to map functional columns if large-vessel contribution to the mapping signals can be minimized.

Confirmation of Columnar-Resolution fMRI Maps

Even though column-like functional structures were mapped, it is not known whether higher CBF and CBV changes indicate neuronally active columns. When a single cortical column is activated, the highest fMRI signal will appear at the site of increased neuronal activity regardless of its PSF. However, when multiple columns are activated, successfully determining the location of active columns within fMRI maps will be dictated by the PSF width relative to the distance between neighboring active columns. Because of this limitation, it is conceivable that the highest CBV signals induced by bars of 0° (90°) orientation may appear at the location of 90° (0°) orientation columns. Thus, it is essential to confirm our fMRI observation using optical images with known neural correlates because a good correlation between neural activity and OIS has already been observed in the visual cortex (Grinvald and others 1986; Shmuel and Grinvald 1996; Maldonado and others 1997; Bosking and others 2002). To achieve high sensitivity for orientation column mapping, we used CBV-weighted fMRI with iron oxide nanoparticles and the continuous stimulation paradigm. After fMRI data collection, OIS experiments were performed with the same stimulation paradigm on the same animal (Fukuda and others 2006a).

Functional MRI and optical images were coregistered using pial vessel patterns; because the slice chosen for fMRI studies was below the cortical surface, the pial vessel pattern above the fMRI slice was visualized using a 2-D MR image. Then, the optical image was linearly transformed manually so that pial vessel patterns matched the MRI patterns. Because functional signals were obtained during an 80-s cyclical stimulation, the peak of the functional response specific to a particular orientation can therefore be observed every 80 s (Fig. 7). Thus, this orientation-specific signal was extracted by selecting the orientation-specific stimulation frequency component in Fourier analysis. The non-orientation-specific signal induced by each stimulus presentation is almost saturated by continuous stimulation. Dark patches in fMRI maps have larger CBV changes responding to a presented orientation, and dark patches in optical images indicate active sites responding to a presented orientation (see Fig. 8). Iso-orientation maps of fMRI were similar to those of OIS; activation borders, columnar patterns (black and white patches and bands), and most loci show a good match between the 2 modalities. Thus, the highest CBV-weighted fMRI signal change is expected at the site of increased neuronal activity.

All human columnar mapping has been demonstrated using positive BOLD signals (Menon and others 1997; Menon and Goodyear 1999; Dechent and Frahm 2000; Cheng and others 2001; Goodyear and Menon 2001). Because the BOLD PSF is determined by a mismatch between $CMRO_2$ and CBF responses, its assignment of neural activity sites into BOLD columnar maps is not clear. When multiple columns are active, the highest BOLD signals could originate from neurally active domains if CBF PSF is narrow relative to an intercolumn distance (Duong and others 2001), or the highest BOLD signal could originate from neurally inactive domains if the CBF response is broad, as suggested by optical spectroscopic imaging (Malonek and Grinvald 1996). To evaluate whether the highest BOLD response occurs in the active columns, we used CBV-related fMRI maps as a reference, where spatial neural correlations are known (Fukuda and others 2006a). Orientation-specific modulations of the 80-s cycle are again extracted by Fourier analysis (Fig. 7). The orientation-specific modulation of 1/80 Hz for the BOLD signal begins at a positive deflection and is almost opposite to that of the CBV-weighted signal (Fig. 7*A*; note that a negative CBV-weighted signal indicates an increase in CBV). Iso-orientation maps of the BOLD signal were significantly correlated to those of CBV-weighted fMRI (see Fig. 9). Thus, the highest orientation-selective

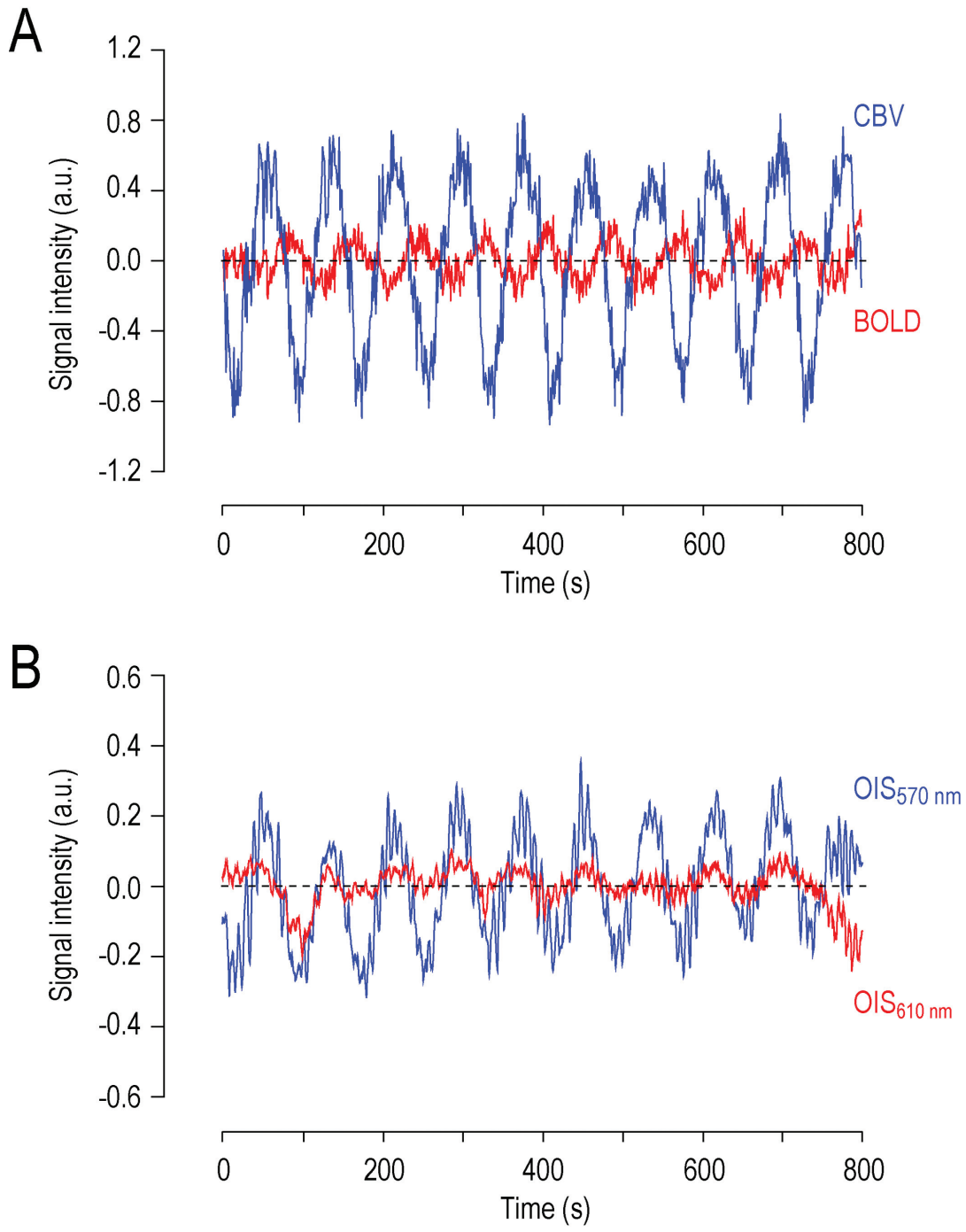

Fig. 7. Orientation-selective modulations during 800-s continuous stimulation. Eight 10-s long orientation-selective stimuli starting at 0° and increasing 22.5° were repeated 10 times. Cerebral blood volume (CBV)–weighted (blue) and deoxyhemoglobin (dHb)–weighted (red) fMRI signals (*A*) and optimal imaging of intrinsic (OIS) responses (*B*) were obtained from 0°-specific columns. In optical imaging (*B*), a reflected response of a 570-nm wavelength light is weighted by CBV, whereas that of the 610-nm wavelength is weighted by dHb. A decrease in CBV- and dHb-weighted signal indicates an increase in CBV and dHb, respectively. In both fMRI and OIS data, orientation-selective stimulation induces a decrease in CBV-weighted signals (i.e., an increase in CBV). Blood oxygenation level–dependent (BOLD) response increases during orientation-selective stimulation, whereas the 610-nm OIS response decreases. The time to peak of CBV and BOLD response slightly differs due to their different response characteristics.

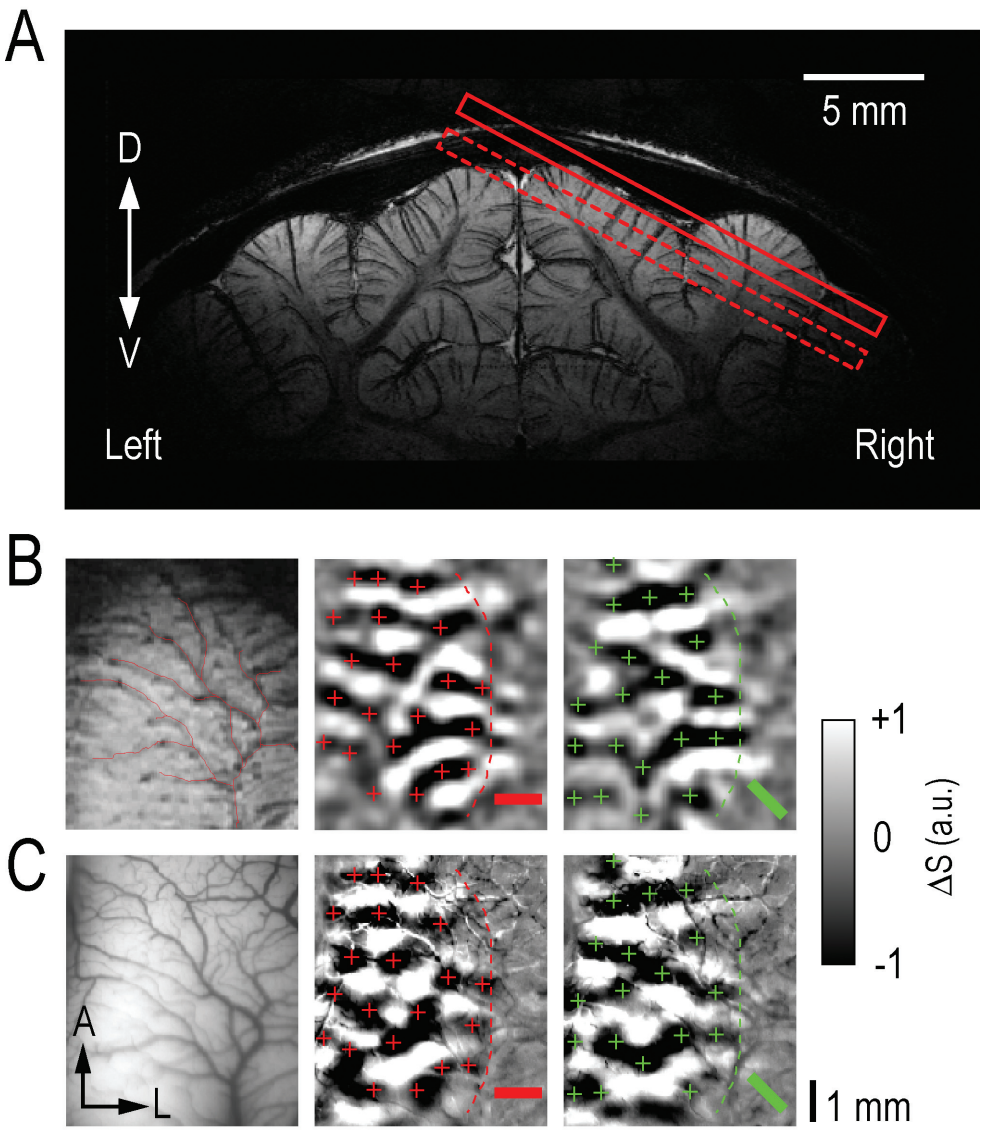

Fig. 8. Comparison between CBV-weighted fMRI and optical images (Fukuda and others 2006a). An fMRI slice was selected in the middle of the cortex through the gyrus in the right hemisphere (indicated as a dashed slab), whereas optical imaging was obtained from the upper cortical layers, including the surface of the cortex. Thus, to coregister both modality images, pial vessel patterns just above the fMRI slice (indicated as a solid slab in *A*) were compared with the optical image (*B* vs. *C*). Functional maps were obtained from continuous stimulation and Fourier analysis. In the functional maps, dark patches represent the region preferentially responding to the orientation stimulus shown in the right corner, whereas white patches represent orthogonal orientation stimulation. Plus signs were marked based on fMRI patches and overlaid on optical maps. Clearly, fMRI and optical images agree very well. D = dorsal; V = ventral.

BOLD signals indicate the sites of increased neural activity. In other words, the magnitude of BOLD response to preferred stimulation should be larger than the magnitude of response to nonpreferred stimulation (Moon and others 2007).

Column-Specific BOLD versus dHb-Weighted OIS Signals

Although a good match of orientation column maps between fMRI and optical imaging was observed, a

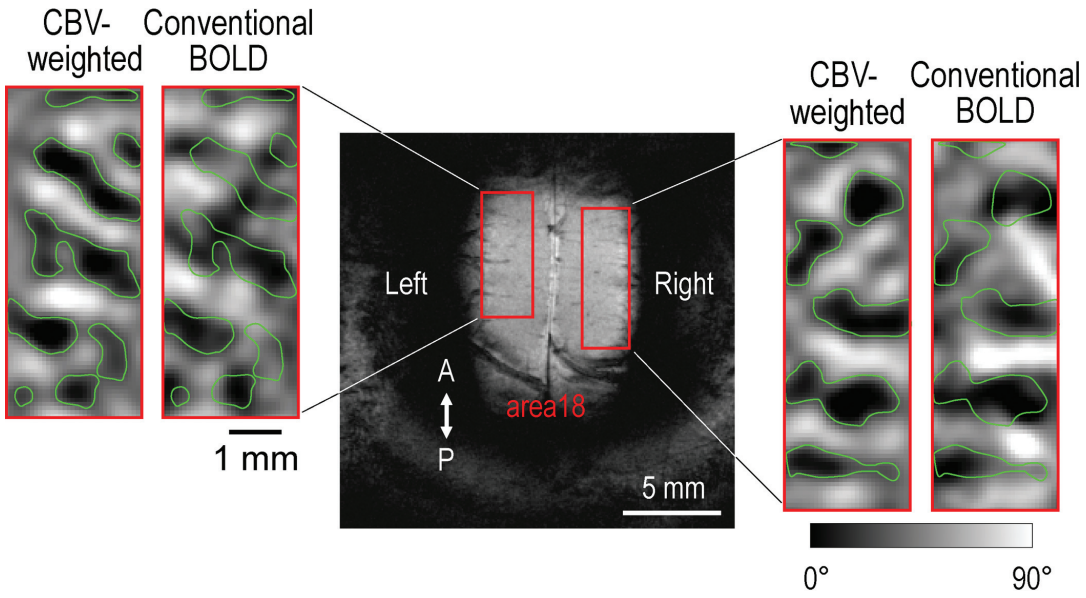

Fig. 9. Cerebral blood volume (CBV)–weighted versus blood oxygenation level–dependent (BOLD) fMRI. CBV-weighted fMRI followed conventional BOLD fMRI. Both maps were determined from continuous stimulation data and Fourier analysis. Higher signal change responding to 0° stimulation appears as black, whereas that responding to 90° appears white. Gray indicates either a 45° or 135° response area. Green contours indicating 0° columns were marked based on CBV-weighted fMRI and overlaid on fMRI maps. Even though some regions mismatch between CBV-weighted and BOLD fMRI, there is generally good agreement between the 2 modalities. A = anterior; P = posterior.

discrepancy in orientation-specific modulation was seen between the BOLD and dHb-weighted intrinsic signal (Fig. 7). Our results (see Figs. 7, 9) clearly demonstrate that the preferred stimulation induces a larger positive BOLD signal than the nonpreferred stimulation. Thus, dHb content should decrease more during the preferred stimulation than during the nonpreferred stimulation (i.e., more hyperoxygenation during the preferred stimulation). In contrast, the orientation-specific dHb-weighted OIS signal begins at a negative deflection as similar to the CBV-weighted OIS signal (Fig. 7B; note that negative reflected 570-nm signal indicates an increase in CBV). This result implies that the preferred stimulation induces a smaller decrease in the dHb amount than the nonpreferred stimulation (i.e., less hyperoxygenation during the preferred stimulation) (Malonek and Grinvald 1996; Grinvald and others 2000; Fukuda and others 2005). What causes this apparent contradiction of the supposed dHb signals between fMRI and optical imaging?

When the CBF and CBV responses induced by neural activity are minimal at the vasodilator-induced hypotension condition (Nagaoka and others 2006), similar to the condition of the early dip, both the negative BOLD signal (Fukuda and others 2006a) and the optical imaging signal (Fukuda and others 2006b) have similarly larger hypooxygenated changes at active columns than inactive columns. This indicates that the dHb contribution is dominant in both BOLD and optical imaging signals when CBF and CBV responses are minimal. This suggests that the difference between BOLD and optical imaging signals at the normal condition appears to relate to CBF and/or CBV responses, which requires further systematic studies.

Conclusions

We hope our studies have helped to confirm that fMRI can convincingly map functional cortical columns. Both BOLD and CBV techniques can be used to determine functional columnar structure in cortical areas, which have not been investigated previously, such as regions deeply embedded in sulci (Fig. 10) or possibly on a layer-to-layer basis. Also, a plastic and/or developmental change of functional columns can be noninvasively tracked. Because sensitivity of the CBV-weighted fMRI signal is higher than that of the BOLD fMRI, CBV-weighted fMRI with contrast agent is preferable in animal studies.

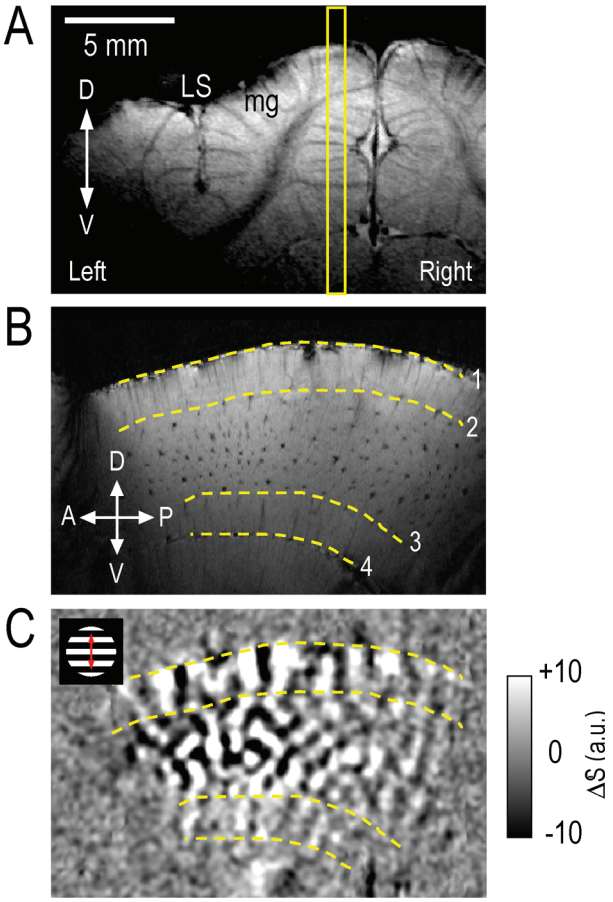

Fig. 10. Cerebral blood volume (CBV)–weighted fMRI map in the medial region (Fukuda and others 2006a). CBV-weighted fMRI was obtained on a sagittal imaging slice in the medial bank of cortical area 17 (*A*) with a continuous stimulation paradigm. The vessel-weighted sagittal image (*B*) shows orientations of intracortical veins relative to the imaging slice; dark lines indicate vessels run within the imaging slice (as indicated between lines 1–2 and 3–4), whereas dark spots indicate vessels run through the imaging slice (lines 2–3). Spatially distinct activation patterns appear as irregular patches and bands. Patchy patterns appear in the region between dashed lines 2 and 3, where the imaging plane is parallel to the cortical surface. Band-shaped patterns appear in regions where the imaging plane is perpendicular to the cortical surface (between dashed lines 1 and 2, as well as between lines 3 and 4). LS = lateral sulcus; mg = marginal gyrus; D = dorsal; V = ventral; A = anterior; P = posterior.

References

Ances BM, Buerk DG, Greenberg JH, Detre JA. 2001. Temporal dynamics of the partial pressure of brain tissue oxygen during functional forepaw stimulation in rats. Neurosci Lett 306:106–10.

Blasdel G. 1992. Differential imaging of ocular dominance and orientation selectivity in monkey striate cortex. J Neurosci 12:3115–38.

Blasdel G, Salama G. 1986. Voltage-sensitive dyes reveal a modular organization in monkey striate cortex. Nature 321:579–85.

Bonhoeffer T, Grinvald A. 1991. Iso-orientation domains in cat visual cortex are arranged in pinwheel-like pattern. Nature 353:429–32.

Bonhoeffer T, Grinvald A. 1993. The layout of iso-orientation domains in area 18 of cat visual cortex: optical imaging reveals a pin-wheel-like organization. J Neurosci 13:4157–80.

Bosking W, Crowley J, Fitzpatrick D. 2002. Spatial coding of position and orientation in primary visual cortex. Nat Neurosci 5:874–82.

Cheng K, Waggoner R, Tanaka K. 2001. Human ocular dominance columns as revealed by high-field functional magnetic resonance imaging. Neuron 32:359–74.

Das A, Gilbert C. 1995. Long-range horizontal connections and their role in cortical reorganization revealed by optical recording of cat primary visual cortex. Nature 375:780–4.

Dechent P, Frahm J. 2000. Direct mapping of ocular dominance columns in human primary visual cortex. Neuroreport 11:3247–9.

Detre JA, Leigh JS, Williams DS, Koretsky AP. 1992. Perfusion imaging. Magn Reson Med 23:37–45.

Duong TQ, Kim D-S, Ugurbil K, Kim S-G. 2000. Spatio-temporal dynamics of the BOLD fMRI signals: toward mapping submillimeter columnar structures using the early negative response. Magn Reson Med 44:231–42.

Duong TQ, Kim D-S, Ugurbil K, Kim S-G. 2001. Localized cerebral blood flow response at submillimeter columnar resolution. Proc Natl Acad Sci USA 98:10904–9.

Duvernoy H, Delon S, Vannson J. 1981. Cortical blood vessels of the human brain. Brain Res Brain 7:519–79.

Edelman RR, Siewert B, Darby DG, Thangaraj V, Nobre AC, Mesulam MM, and others. 1994. Qualitative mapping of cerebral blood flow and functional localization with echo-planar MR imaging and signal targeting with alternating radio frequency. Radiology 192:513–20.

Engel A, Glover G, Wendell B. 1997. Retinotopic organization in human visual cortex and the spatial precision of functional MRI. Cereb Cortex 7:181–92.

Fox PT, Raichle ME. 1986. Focal physiological uncoupling of cerebral blood flow and oxidative metabolism during somatosensory stimulation in human subjects. Proc Natl Acad Sci USA 83:1140–4.

Fox PT, Raichle ME, Mintun MA, Dence C. 1988. Nonoxidative glucose consumption during focal physiologic neural activity. Science 241:462–4.

Frostig RD, Lieke EE, Ts'o DY, Grinvald A. 1990. Cortical functional architecture and local coupling between neuronal activity and the microcirculation revealed by in vivo high-resolution optical imaging of intrinsic signals. Proc Natl Acad Sci USA 87:6082–6.

Fukuda M, Moon C-H, Wang P, Kim S-G. 2006a. Mapping iso-orientation columns by contrast agent-enhanced functional MRI: reproducibility, specificity and evaluation by optical imaging of intrinsic signal. J Neurosci 26:11821–32.

Fukuda M, Rajagopalan UM, Homma R, Matsumoto M, Nishizaki M, Tanifuji M. 2005. Localization of activity-dependent changes in blood volume to submillimeter-scale functional domains in cat visual cortex. Cereb Cortex 15:823–33.

Fukuda M, Wang P, Moon CH, Tanifuji M, Kim S-G. 2006b. Spatial specificity of the enhanced dip inherently induced by prolonged oxygen consumption in cat visual cortex: implication for columnar resolution functional MRI. Neuroimage 30:70–87.

Goodyear B, Menon RS. 2001. Brief visual stimulation allows mapping of ocular dominance in visual cortex using fMRI. Human Brain Mapping 14:210–7.

Grinvald A. 1992. Optical imaging of architecture and function in the living brain sheds new light on cortical mechanisms underlying visual perception. Brain Topogr 5:71–5.

Grinvald A, Leike E, Frostig RD, Gillbert CD, Wiesel TN. 1986. Functional architecture of cortex revealed by optical imaging of intrinsic signals. Nature 324:361–4.

Grinvald A, Slovin H, Vanzetta I. 2000. Non-invasive visualization of cortical columns by fMRI. Nat Neurosci 3:105–7.

Heeger DJ, Huk AC, Geisler WS, Albrecht DG. 2000. Spikes versus BOLD: what does neuroimaging tell us about neuronal activity? Nat Neurosci 3:631–3.

Horton J, Adams D. 2005. The cortical column: a structure without a function. Philos Trans R Soc Lond B Biol Sci 360:837–62.

Hubel D, Wiesel T. 1962. Receptive fields, binocular interactions and functional architecture in the cat's visual cortex. J Physiol London 160:106–54.

Hubel D, Wiesel T. 1963. Shape and arrangement of columns in cat's striate cortex. J Physiol London 165:559–68.
Kalatsky V, Stryker MP. 2003. New paradigm for optical imaging: temporally encoded maps of intrinsic signal. Neuron 38:529–45.
Kennan RP, Scanley BE, Innis RB, Gore JC. 1998. Physiological basis for BOLD MR signal changes due to neuronal stimulation: separation of blood volume and magnetic susceptibility effects. Magn Reson Med 40:840–6.
Kennedy C, Des Rosiers MH, Sakurada O. 1976. Metabolic maps of the primary visual system of the monkey by means of autoradiographic ^{14}C-deoxyglucose technique. Proc Natl Acad Sci USA 73:4230–4.
Kim D-S, Duong TQ, Kim S-G. 2000. High-resolution mapping of iso-orientation columns by fMRI. Nat Neurosci 3:164–9.
Kim D-S, Ronen I, Olman C, Kim SG, Ugurbil K, Toth LJ. 2004. Spatial relationship between neuronal activity and BOLD functional MRI. Neuroimage 21:876–85.
Kim S-G. 1995. Quantification of relative cerebral blood flow change by flow-sensitive alternating inversion recovery (FAIR) technique: application to functional mapping. Magn Reson Med 34:293–301.
Kim S-G, Hendrich K, Hu X, Merkle H, Ugurbil K. 1994. Potential pitfalls of functional MRI using conventional gradient-recalled echo techniques. NMR Biomed 7:69–74.
Kim S-G, Ugurbil K. 2003. High-resolution functional magnetic resonance imaging of the animal brain. Sci Direct Methods 30:28–41.
Kwong KK, Chesler DA, Weisskoff RM, Donahue KM, Davis TL, Ostergaard L, and others. 1995. MR perfusion studies with T1-weighted echo planar imaging. Magn Reson Med 34:878–87.
Lee AT, Glover GH, Meyer CH. 1995. Discrimination of large venous vessels in time-course spiral blood-oxygen-level-dependent magnetic-resonance functional neuroimaging. Magn Reson Med 33:745–54.
Lee S-P, Duong T, Yang G, Iadecola C, Kim S-G. 2001. Relative changes of cerebral arterial and venous blood volumes during increased cerebral blood flow: implications for BOLD fMRI. Magn Reson Med 45:791–800.
Leenders KL, Perani D, Lammertsma AA, Heather JD, Buckingham P, Jones T, and others. 1990. Cerebral blood flow, blood volume and oxygen utilization. Brain 113:27–47.
Logothetis NK, Pauls J, Augath M, Trinath T, Oeltermann A. 2001. Neurophysiological investigation of the basis of the fMRI signal. Nature 412:150–7.
Lowel S, Bischof H, Leutenecker B, Singer W. 1988. Topographic relations between ocular dominance and orientation columns in the cat striate cortex. Exp Brain Res 71:33–46.
Lowel S, Freeman B, Singer W. 1987. Topographic organization of the orientation column system in large flat-mounts of the cat visual cortex: a 2-deoxyglucose study. J Comp Neurol 255:401–15.
Malach R, Amir Y, Harel M, Grinvald A. 1993. Relationship between intrinsic connections and functional architecture revealed by optical imaging and in vivo targeted biocytin injections in primate striate cortex. Proc Natl Acad Sci USA 90:469–73.
Maldonado PE, Goedecke I, Gray CM, Bonhoeffer T. 1997. Orientation selectivity in pinwheel centers in cat visual cortex. Science 276:1551–5.
Malonek D, Grinvald A. 1996. Interactions between electrical activity and cortical microcirculation revealed by imaging spectroscopy: implication for functional brain mapping. Science 272:551–4.
Mandeville JB, Jenkins BG, Kosofsky BE, Moskowitz MA, Rosen BR, Marota JJA. 2001. Regional sensitivity and coupling of BOLD and CBV changes during stimulation of rat brain. Magn Reson Med 45:443–7.
Mandeville JB, Marota JJA. 1999. Vascular filters of functional MRI: spatial localization using BOLD and CBV contrast. Magn Reson Med 42:591–8.
Mandeville JB, Marota JJA, Kosofsky BE, Keltner JR, Weissleder R, Rosen BR. 1998. Dynamic functional imaging of relative cerebral blood volume during rat forepaw stimulation. Magn Reson Med 39:615–24.
Mayhew JE, Askew S, Zheng Y, Porrill J, Westby G, Redgrave P, and others. 1996. Cerebral vasomotion: a 0.1-Hz oscillation in reflected light imaging of neural activity. Neuroimage 4:183–93.
Menon RS, Goodyear BG. 1999. Submillimeter functional localization in human striate cortex using BOLD contrast at 4 Tesla: implications for the vascular point-spread function. Magn Reson Med 41:230–5.
Menon RS, Ogawa S, Strupp JP, Ugurbil K. 1997. Ocular dominance in human V1 demonstrated by functional magnetic resonance imaging. J Neurophysiol 77:2780–7.
Moon CH, Fukuda M, Park SH, Kim SG. 2007. Neural interpretation of blood oxygenation level dependent fMRI at submillimeter columnar resolution. J Neurosci 27:6892–902.
Mountcastle V. 1957. Modality and topographic properties of single neurons of cat's somatic sensory cortex. J Neurophysiol 20:408–34.
Movshon JA, Thompson ID, Tolhurst DJ. 1978. Spatial and temporal contrast sensitivity of neurons in areas 17 and 18 of the cat's visual cortex. J Physiol 283:101–20.
Nagaoka T, Zhao F, Wang P, Harel N, Kennan RP, Ogawa S, and others. 2006. Increases in oxygen consumption without cerebral blood volume change during visual stimulation under hypotension condition. J Cereb Blood Flow Metab 26:1043–51.
Ogawa S, Lee TM. 1990. Magnetic resonance imaging of blood vessels at high fields: in vivo and in vitro measurements and image simulation. Magn Reson Med 16:9–18.
Ogawa S, Lee T-M, Kay AR, Tank DW. 1990a. Brain magnetic resonance imaging with contrast dependent on blood oxygenation. Proc Natl Acad Sci USA 87:9868–72.
Ogawa S, Lee T-M, Nayak AS, Glynn P. 1990b. Oxygenation-sensitive contrast in magnetic resonance image of rodent brain at high magnetic fields. Magn Reson Med 14:68–78.
Ogawa S, Menon RS, Tank DW, Kim S-G, Merkle H, Ellermann JM, and others. 1993. Functional brain mapping by blood oxygenation level-dependent contrast magnetic resonance imaging. Biophys J 64:800–12.
Pauling L, Coryell CD. 1936. The magnetic properties and structure of hemoglobin, oxyhemoglobin and carbonmonoxyhemoglobin. Proc Natl Acad Sci USA 22:210–6.
Pawlik G, Rackl A, Bing RJ. 1981. Quantitative capillary topography and blood flow in the cerebral cortex of cats: an in vivo microscopic study. Brain Res 208:35–58.
Payne BR, Peters A. 2002. The concept of cat primary visual cortex. In: Payne BR, Peters A, editors. The Cat Primary Visual Cortex. New York: Academic Press. p 1–129.
Purves D, Riddle D, LaMantia A-S. 1992. Iterated patterns of brain circuitry. Trends Neurosci 15:362–8.
Shibuki K, Hishida R, Murakami H, Kudoh M, Kawaguchi T, Watanabe M, and others. 2003. Dynamic imaging of somatosensory cortical activity in the rat visualized by flavoprotein autofluorescence. J Physiol 549:919–27.
Shmuel A, Grinvald A. 1996. Functional organization for direction of motion and its relationship to orientation maps in cat area 18. J Neurosci 16:6945–64.
Swindale N. 1990. Is the cerebral cortex modular? Trends Neurosci 13:487–92.
Thompson JK, Peterson MR, Freeman RD. 2003. Single-neuron activity and tissue oxygenation in the cerebral cortex. Science 299:1070–2.
Tso DY, Frostig RD, Lieke EE, Grinvald A. 1990. Functional organization of primate visual cortex revealed by high resolution optical imaging. Science 249:417–20.
van Bruggen N, Busch E, Palmer JT, Williams S-P, de Crespigny AJ. 1998. High-resolution functional magnetic resonance imaging of the rat brain: mapping changes in cerebral blood volume using iron oxide contrast media. J Cereb Blood Flow Metab 18:1178–83.
Vanduffel W, Fize D, Mandeville JB, Nelissen K, van Hecke P, Rosen BR, and others. 2001. Visual motion processing investigated using contrast agent-enhanced fMRI in awake behaving monkeys. Neuron 32:565–77.
Vanzetta I, Grinvald A. 1999. Cortical activity-dependent oxidative metabolism revealed by direct oxygen tension measurements: implications for functional brain imaging. Science 286:1555–8.
Zhao F, Wang P, Hendrich K, Kim S-G. 2005a. Mapping cat visual orientation columns using CBV-weighted fMRI. Presented at the Proc 13th Annual Meeting, ISMRM, Miami, FL.
Zhao F, Wang P, Hendrich K, Kim S-G. 2005b. Spatial specificity of cerebral blood volume-weighted fMRI responses at columnar resolution. Neuroimag 27:416–24.
Zhao F, Wang P, Hendrich K, Ugurbil K, Kim S-G. 2006. Cortical layer-dependent BOLD and CBV responses measured by spin-echo and gradient-echo fMRI: insights into hemodynamic regulation. Neuroimage 30:1149–60.